Cellular/Molecular

# Repolarizing Responses of $BK_{Ca}$–Cav Complexes Are Distinctly Shaped by Their Cav Subunits

**Henrike Berkefeld and Bernd Fakler**
Institute of Physiology, University of Freiburg, 79104 Freiburg, Germany

**Large-conductance $Ca^{2+}$- and voltage-activated potassium ($BK_{Ca}$) channels shape the firing pattern in many types of excitable cell through their repolarizing $K^+$ conductance. The onset and duration of the $BK_{Ca}$-mediated currents typically initiated by action potentials (APs) appear to be cell-type specific and were shown to vary between 1 ms and up to a few tens of milliseconds. In recent work, we showed that reliable activation of $BK_{Ca}$ channels under cellular conditions is enabled by their integration into complexes with voltage-activated $Ca^{2+}$ (Cav) channels that provide $Ca^{2+}$ ions at concentrations sufficiently high ($\geq$10 $\mu$M) for activation of $BK_{Ca}$ in the physiological voltage range. Formation of $BK_{Ca}$–Cav complexes is restricted to a subset of Cav channels, Cav1.2 (L-type) and Cav2.1/2.2 (P/Q- and N-type), which differ greatly in their expression pattern and gating properties. Here, we reconstituted distinct $BK_{Ca}$–Cav complexes in *Xenopus* oocytes and culture cells and used patch-clamp recordings to compare the functional properties of $BK_{Ca}$–Cav1.2 and $BK_{Ca}$–Cav2.1 complexes. Under steady-state conditions, $K^+$ currents mediated by $BK_{Ca}$–Cav2.1 complexes exhibit a considerably faster rise time and reach maximum at potentials markedly more negative than complexes formed by $BK_{Ca}$ and Cav1.2, in line with the distinct steady-state activation and gating kinetics of the two Cav subtypes. When AP waveforms were used as a voltage command, $K^+$ currents mediated by $BK_{Ca}$–Cav2.1 occurred at shorter APs and lasted longer than that of $BK_{Ca}$–Cav1.2. These results demonstrate that the repolarizing $K^+$ currents through $BK_{Ca}$–Cav complexes are shaped by the respective Cav subunit and that the distinct Cav channels may adapt $BK_{Ca}$ currents to the particular requirements of distinct types of cell.**

*Key words:* **$Ca^{2+}$-activated $K^+$ channels; Cav channels; $BK_{Ca}$ channels; calcium signaling; action potential; potassium channel**

## Introduction

Large-conductance calcium- and voltage-activated $K^+$ channels (also termed $BK_{Ca}$, $K_{Ca}1.1$, or Slo1) act as key modulators of electrical signaling in many types of excitable cell (Sah and Faber, 2002; Latorre and Brauchi, 2006). Activated by the concerted action of membrane depolarization and elevation in intracellular $Ca^{2+}$ concentration ($[Ca^{2+}]_i$) $BK_{Ca}$ channels provide the robust $K^+$ currents that contribute to action potential (AP) repolarization (Storm, 1987b; Edgerton and Reinhart, 2003), mediate the fast phase of afterhyperpolarization (fAHP) (Lancaster and Nicoll, 1987; Storm, 1987a; Yazejian et al., 2000), shape dendritic $Ca^{2+}$ spikes (Golding et al., 1999; Rancz and Häusser, 2006), and influence transmitter release (Robitaille et al., 1993). Both onset and duration of the $BK_{Ca}$-mediated $K^+$ currents vary widely among different cell types or among different subcellular compartments (Hu et al., 2001; Pattillo et al., 2001). Thus, in cerebellar Purkinje cells and hippocampal granule and pyramidal cells (Shao et al., 1999; Edgerton and Reinhart, 2003; Loane et al., 2007; Müller et al., 2007), $BK_{Ca}$ channels are activated by short APs and remain open for a few milliseconds, whereas in chromaffin cells, vomeronasal sensory neurons, suprachiasmatic nucleus neurons, and smooth muscle cells the periods of channel activity extend to a few tens of milliseconds (Heppner et al., 1997; Lovell and McCobb, 2001; Jackson et al., 2004; Ukhanov et al., 2007).

Mechanistically, membrane depolarization and elevation in $[Ca^{2+}]_i$ converge allosterically on the gating machinery of $BK_{Ca}$ channels, with increasing $Ca^{2+}$ concentrations shifting the steady-state activation curve into the physiological voltage range (Marty, 1981; Cui et al., 1997). Robust activation of $BK_{Ca}$ channels at potentials $\leq$20 mV requires values for $[Ca^{2+}]_i$ of $\geq$10 $\mu$M, which in the cellular context may be achieved either by a global or local/focal rise in $[Ca^{2+}]_i$. In CNS neurons and most other cell types, high micromolar levels of $[Ca^{2+}]_i$ are restricted to so-called "$Ca^{2+}$-nano/microdomains" that form around active $Ca^{2+}$ sources, particularly voltage-gated $Ca^{2+}$ (Cav) channels (Neher, 1998; Augustine et al., 2003). In recent work using functional proteomics, we showed that $BK_{Ca}$ channels in the rat brain, tetramers of $\alpha$ subunits (BK$\alpha$) either alone or together with the auxiliary subunits BK$\beta$2/4 (Berkefeld et al., 2006), are able to coassemble with a subset of Cav channels into macromolecular $BK_{Ca}$–Cav complexes placing both types of channel within nanometers of each other. Within these complexes, $BK_{Ca}$ channels are supplied with $[Ca^{2+}]_i$ sufficiently high to ensure robust channel activation at physiological membrane potentials with onset of $BK_{Ca}$ currents after Cav channel activation by less than a millisecond (Berkefeld et al., 2006). Moreover, this coupling exhibits the distinct sensitivity to $Ca^{2+}$ buffers defining for $Ca^{2+}$ nanodo-

Received July 9, 2008; revised June 25, 2008; accepted July 1, 2008.

This work was supported by Deutsche Forschungsgemeinschaft Grant Fa 332/5-3 (B.F.). We thank J. P. Adelman for his advice and critical reading of this manuscript.

Correspondence should be addressed to Bernd Fakler, Institute of Physiology, University of Freiburg, Hermann-Herder-Strasse 7, 79104 Freiburg, Germany. E-mail: bernd.fakler@physiologie.uni-freiburg.de.

DOI:10.1523/JNEUROSCI.2274-08.2008

 0270-6474/08/288238-08$15.00/0

mains: it can be interfered with the fast chelator BAPTA, whereas EGTA is entirely ineffective.

The Cav channels that physically interact with $BK_{Ca}$ through their $\alpha$-subunits are Cav1.2 (L-type), Cav2.1 (P/Q-type), and Cav2.2 (N-type) (Berkefeld et al., 2006). These Cav subtypes are greatly distinct with respect to cellular distribution, subcellular localization, and functional properties. Thus, Cav2.1 and Cav2.2 are predominantly found in the synaptic compartment (Kulik et al., 2004), where they are crucial for neurotransmitter release (Castillo et al., 1994; Wu et al., 1999; Pelkey et al., 2006). In contrast, Cav1.2 channels are mostly localized in cell somata and dendrites (Reid et al., 2003; Obermair et al., 2004), in which they are involved in the control of bioelectrical regenerative properties (Dobremez et al., 2005).

The present work investigated the impact of distinct Cav subtypes on the characteristics of the repolarizing $K^+$ current output of $BK_{Ca}$–Cav complexes in response to voltage steps and AP commands. For this purpose, defined channel–channel complexes composed of $BK_{Ca}$ and either Cav2.1 or Cav1.2 channels were heterologously reconstituted and analyzed by giant and conventional patch-clamp recordings.

## Materials and Methods

*Molecular biology and reconstitution of protein complexes.* $BK_{Ca}$–Cav complexes were heterologously reconstituted in *Xenopus* oocytes and Chinese hamster ovary (CHO) cells by injection of cRNAs or transfection of cDNAs coding for the subunits of $BK_{Ca}$ (BK$\alpha$, BK$\beta$4) and Cav channels (Cav2.1 or 1.2, Cav$\beta$3 or Cav$\beta$1b, $\alpha 2\delta$). Preparation and injection of cRNA into *Xenopus* oocytes were done as described previously (Fakler et al., 1995). Briefly, *Xenopus* oocytes were surgically removed from adult females and manually dissected. Dumont stage VI oocytes were injected with aquatic solution containing the aforementioned cRNAs, treated with collagenase type II 2–3 d after injection, and incubated at 18°C for another 1–3 d before use. CHO cells were transfected with the JetPEI transfection reagent (Biomol), incubated at 37°C and 5% $CO_2$, and measured 2–3 d after transfection. GenBank accessions of the clones used are A48206 (BK$\alpha$, gift from Dr. L. Salkoff, School of Medicine, Washington University, St. Louis, MO), NM_021452.1 (BK$\beta$4), M67515.1 (Cav1.2), NM_017346.1 (Cav$\beta$1b), X57477.1 [Cav2.1(I1520H), gift from Dr. J. Yang, Columbia University, New York, NY], NM_012828.1 (Cav$\beta$3), and AF286488.1 ($\alpha 2\delta$). EGFP was simultaneously added as positive transfection control. All cDNAs were verified by sequencing.

*Electrophysiology.* Standard whole-cell patch-clamp recordings on CHO cells were done at room temperature (22–24°C) as described previously (Bildl et al., 2004). Briefly, currents were recorded with an Axopatch 200B amplifier, filtered at 10 kHz and sampled at 25 kHz. All voltage stimuli were performed as P/4 protocols. Recording pipettes were made from quartz glass capillaries and had resistances of 1–5 MΩ when filled with intracellular solution containing (in mM) 135 KCl, 3.5 $MgCl_2$, 2.5 NaATP, 5 $K_2$EGTA, and 5 HEPES, pH adjusted to 7.3 with HCl. The extracellular solution was composed of (in mM) 144 NaCl, 5.8 KCl, 0.9 $MgCl_2$, 1.3 $CaCl_2$, 0.7 $NaH_2PO_4$, 5.6 D-glucose, and 10 HEPES, pH adjusted to 7.4 with NaOH. Recordings from giant patches excised from *Xenopus* oocytes were performed at room temperature as described previously (Fakler et al., 1995). Briefly, currents were recorded with an EPC9 amplifier (HEKA Elektronik), low-pass filtered at 3 kHz, and sampled at 25 kHz. Pipettes were made from thick-walled borosilicate glass and had resistances of 0.3–0.8 MΩ when filled with (in mM) 115 NaMES, 5 KMES, 10 HEPES, and 1.3 $CaCl_2$, pH adjusted to 7.2 with HMES. Intracellular solution applied via a gravity-driven multibarrel pipette was composed of (in mM) 120 KMES, 5 $K_2$EGTA, and 5 HEPES, pH adjusted to 7.2 with HMES. The bath solution contained (in mM) 120 KMES, 5 HEPES, 1 $K_2$EGTA, and 1 $MgCl_2$, pH adjusted to 7.2 with HMES.

*Data analysis.* Data analyses were done with Igor Pro 4.05A on a Macintosh G4. $K^+$ currents mediated by $BK_{Ca}$–Cav complexes were isolated and characterized via tail-current protocols (see Figs. 1*A*, 2*A*, 5*A*), where the current measured instantaneously after the tail step was taken as the relevant "tail current" carried by $K^+$ ions. Current–voltage (*I–V*) relationships of Cav channels (see Fig. 3*B*) were fitted using the following formula:

$$I(V) = P \times V \times ([D - \exp(-V/C)]/[1 - \exp(V/C)])/(1 + \exp[(V_{1/2} - V)/k]), \quad (1)$$

where $P$ is an amplitude factor, $C$ and $D$ determine current rectification and reversal potential, $V_{1/2}$ is voltage required for half-maximal activation, and $k$ is the corresponding slope factor.

Time constants of channel activation (Fig. 3*C*) were derived from monoexponential fits to the rising phase of the recorded $Ca^{2+}$ currents. All data are given as mean ± SEM.

## Results

### Steady-state activation of $BK_{Ca}$ channels is determined by the associated Cav subtype

For characterization of their response properties, distinct $BK_{Ca}$–Cav complexes were heterologously reconstituted; $BK_{Ca}$ channels (composed of BK$\alpha$ and BK$\beta$4, the BK$\beta$ most abundantly coassembled with BK$\alpha$ in rat brain) (Berkefeld et al., 2006) were coexpressed with either Cav2.1 (Cav2.1, Cav$\beta$3, $\alpha 2\delta$) or Cav1.2 channels (Cav1.2, Cav$\beta$1b, $\alpha 2\delta$) in *Xenopus* oocytes and CHO cells, respectively. Figure 1*A* illustrates typical current responses of $BK_{Ca}$–Cav2.1 complexes to step depolarizations recorded in giant inside-out patches from *Xenopus* oocytes under physiological ion conditions and with a high concentration of EGTA (5 mM) present on the cytoplasmic side (to prevent activation of noncomplexed $BK_{Ca}$ channels) (Berkefeld et al., 2006). For voltage steps exceeding the activation threshold of Cav2.1 channels (approximately −30 mV), current responses were biphasic (Fig. 1*A*, inset): an initial inward current carried by $Ca^{2+}$ that was followed by an outwardly directed $K^+$ current as anticipated for activation of $BK_{Ca}$ channels by $Ca^{2+}$ influx through Cav2.1 channels. Accordingly, $Ca^{2+}$ coupling between both channels was mandatory for activation of $BK_{Ca}$ channels in the voltage range from −50 to 70 mV, as seen in control experiments with $BK_{Ca}$ channels devoid of their Cav partners (Fig. 1*B*).

The amplitude of the combined $Ca^{2+}$ and $K^+$ currents through $BK_{Ca}$–Cav2.1 complexes determined under steady-state conditions ($I_{step}$, recorded 90 ms after step depolarization) was strongly voltage dependent and exhibited a bell-shaped *I–V* relationship peaking at potentials between 0 and 10 mV (Fig. 1*B*). A similar bell-shaped *I–V* relationship with a slightly left-shifted peak amplitude was obtained when the sole $K^+$ current component was plotted over the membrane potential (Fig. 1*B*). Experimentally, the $K^+$ current component was isolated by a tail-current protocol stepping the membrane potential to 60 mV at the end of each depolarizing voltage step (Fig. 1*A*, bottom). At this potential, the $Ca^{2+}$ current was extinguished instantaneously because of the curtailed driving force for $Ca^{2+}$ ions (Fig. 3), whereas the outward-going $K^+$ current was transiently enhanced (before it declined to zero because of the ceased $Ca^{2+}$ influx) (Fig. 1*A*). Because the current amplitude recorded right after the tail step directly reflects channel activity at end of the preceding 100 ms depolarization, the $K^+$ current *I–V* relationship may be regarded as steady-state activation curve of $BK_{Ca}$ channels in $BK_{Ca}$–Cav2.1 complexes. Accordingly, the ascending phase of the bell-shaped *I–V* relationship reflects onset and increase in $BK_{Ca}$ channel activity, whereas the descending phase of the $BK_{Ca}$ channel *I–V* corresponds to cessation in channel activity.

These bell-shaped characteristics were repeated for $K^+$ currents through $BK_{Ca}$ channels integrated into complexes with the

L-type channel encoding Cav1.2 (supplemental Fig. 1, available at www.jneurosci.org as supplemental material). As illustrated in Figure 1*C*, the respective activation curve exhibited ascending and descending phases with a peak value at ~30 mV and an onset of the ascending phase at potentials of ~0 mV, both values markedly shifted toward positive voltages compared with $BK_{Ca}$–Cav2.1 complexes.

Next, we investigated the time course of the $K^+$ currents mediated by $BK_{Ca}$ channels integrated into complexes with either of the two Cav subtypes in response to step depolarizations. A modified tail-current protocol was used to both isolate and scan the time course of the $K^+$ current component (Fig. 2*A*, top). Figure 2*A* (middle) illustrates the result of such a "scanning tail-current protocol" obtained with $BK_{Ca}$–Cav2.1 complexes after a step depolarization to 0 mV: after an initial lag phase, $BK_{Ca}$-mediated currents rose continuously, reaching steady-state amplitude after a few tens of milliseconds (Fig. 2*A*, bottom). The time course of the $BK_{Ca}$ current was voltage-dependent (Fig. 2*B*), as was the initial lag phase defined by the interval between voltage step and $K^+$ current exceeding the 2% relative current threshold (Figs. 2*C*,*D*, gray line). Thus, in the voltage range between −20 and 0 mV where $BK_{Ca}$ channels exhibited peak steady-state activity (Figs. 1*B*,*C*), $K^+$ currents followed the voltage step with a delay of ≤1.5 ms and reached ~25% of their maximal amplitude within 4 ms after the depolarization step (Figs. 2*C*,*E*). In contrast, at more positive potentials the lag phase increased to values ≥3 ms (Figs. 2*C*,*E*). When repeated with $BK_{Ca}$ channels in complex with Cav1.2, $K^+$ currents obtained with the scanning tail-current protocol also displayed voltage-dependent increase in current after an initial delay, albeit with slower kinetics (Figs. 2*B*–*E*). Thus, at potentials with peak activity (~30 mV), the $K^+$ currents reached <10% of their maximum after the first 4 ms period, and the lag phase was ≥3 ms (Figs. 2*B*,*D*,*E*).

Together, these data indicated that $BK_{Ca}$ channels exhibit quite distinct activation properties when associated in bimolecular complexes with either Cav2.1 or Cav1.2 channels.

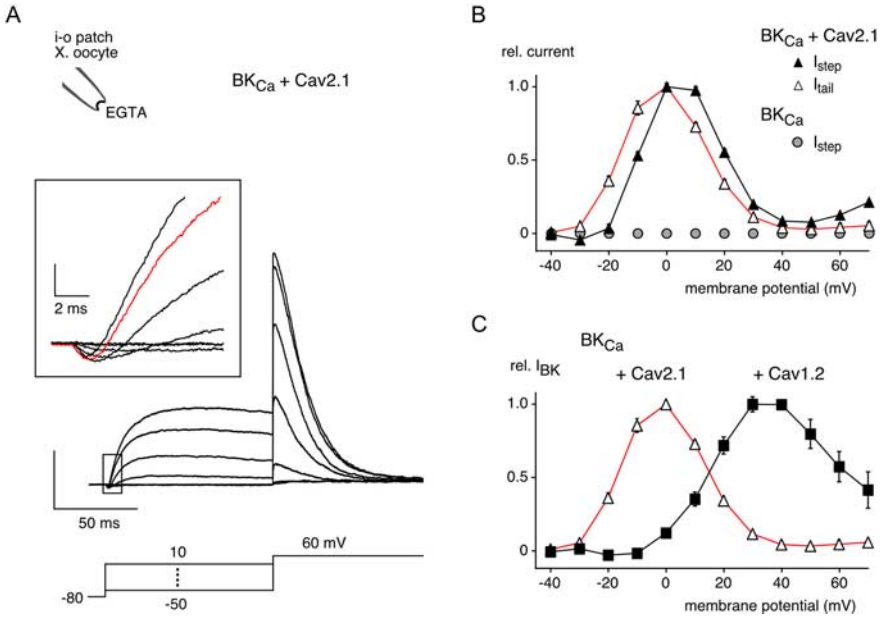


**Figure 1.** Steady-state activation of $BK_{Ca}$ channels is distinct in macromolecular complexes with the Cav subtypes Cav2.1 (P/Q-type) and Cav1.2 (L-type). ***A***, Current response of $BK_{Ca}$–Cav2.1 complexes to the indicated voltage steps (−50 to 10 mV, 10 mV increment, holding potential −80 mV) recorded under physiological ion conditions (1.3 mM extracellular $Ca^{2+}$) in giant inside-out (i–o) patches from *Xenopus* oocytes expressing Cav2.1 [Cav2.1(I1520H), a2$\delta$, Cav$\beta$3] and $BK_{Ca}$ (BK$\alpha$ and BK$\beta$4). Cytoplasmic solution was buffered with 5 mM EGTA (as throughout all experiments). Time scaling is as indicated, and the current scale is 10 nA. Inset, Current traces at expanded time scale (red, current trace at 0 mV). ***B***, Normalized currents through $BK_{Ca}$–Cav2.1 complexes (triangles) or through $BK_{Ca}$ channels alone (circles) as a function of membrane potential recorded from giant i–o patches as in ***A***. Data points are the mean ± SEM of 28 experiments. Filled triangles, Steady-state currents ($I_{step}$) measured 90 ms after the voltage step. Open triangles, Tail currents ($I_{tail}$) measured immediately after voltage step to the tail potential; $I_{tail}$ represents the activation curve of $BK_{Ca}$ channels in $BK_{Ca}$–Cav2.1 complexes. ***C***, Activation curves of $BK_{Ca}$ channels in complexes with either Cav2.1 (triangles, from ***B***) or Cav1.2 channels (squares). Data points for $BK_{Ca}$–Cav1.2 complexes are the mean ± SEM of six experiments. rel., Relative (for all figures).

**Distinct response properties of Cav2.1 and Cav1.2 channels**

We, therefore, analyzed the properties of these two Cav channel subtypes (molecular composition as indicated above) under the same physiological ion conditions as before, in particular using an extracellular $Ca^{2+}$ concentration of 1.3 mM together with 5 mM of the $Ca^{2+}$ chelator EGTA on the cytoplasmic side.

As shown in Figures 3, *A* and *B*, both types of Cav channel provided robust currents in response to step depolarizations and their maximal current amplitudes defined bell-shaped *I–V* relationships with distinct characteristics. Thus, for Cav2.1 channels, the threshold for activation and the peak current amplitude were observed at more negative potentials than for Cav1.2 channels, with values for the voltage generating peak current amplitudes of −10.2 mV (fit to the mean) and 19.3 mV for Cav2.1 and Cav1.2, respectively (Fig. 3*B*). The midpoint potentials (and slope factor) for steady-state activation obtained from fitting Equation 1 to the respective *I–V* relationships were −18.7 ± 1.3 mV (and 5.9 ± 0.4 mV) for Cav2.1 and 7.0 ± 2.5 mV (and 8.1 ± 0.4 mV) for Cav1.2. In addition to steady-state activation, both Cav channels exhibited distinct activation kinetics as indicated by the time constants obtained from monoexponential fits to the current onset (Fig. 3*C*). Thus, for membrane potentials ≥0 mV, activation of Cav2.1 channels was significantly faster ($p \leq 0.01$) than that of Cav1.2 channels, with values for $\tau_{activation}$ ranging from 1.07 ± 0.18 to 0.37 ± 0.08 ms for Cav2.1 and from 1.83 ± 0.24 ms to 0.78 ± 0.07 ms for Cav1.2 channels.

The *I–V* relationships of the two Cav subtypes closely resembled the activation curve of complexed $BK_{Ca}$ channels providing explanation for both its shape and position on the voltage axis (Fig. 3*D*). Thus, onset and ascending phase of the $BK_{Ca}$ currents are determined by the voltage-dependent activation of the associated Cav channels, whereas the descending phase is attributable to the decrease in $Ca^{2+}$ currents; the latter was quite distinct for Cav2.1 and Cav1.2 (see Discussion), as was the decrease of $BK_{Ca}$ currents observed for the respective $BK_{Ca}$–Cav complex (Fig. 3*D*). Together, these results indicated that the Cav channel mainly shapes the current output of $BK_{Ca}$–Cav complexes when voltage steps were used as command inputs.

Native $BK_{Ca}$–Cav complexes are operated by APs. Therefore, we next investigated the responses of Cav channels as well as $BK_{Ca}$–Cav complexes to AP-like voltage commands. Starting from a holding potential of −80 mV, these commands depolarized the membrane potential by a 0.5 ms voltage-ramp to 40 mV, before a subsequent ramp with durations varying between 0.5

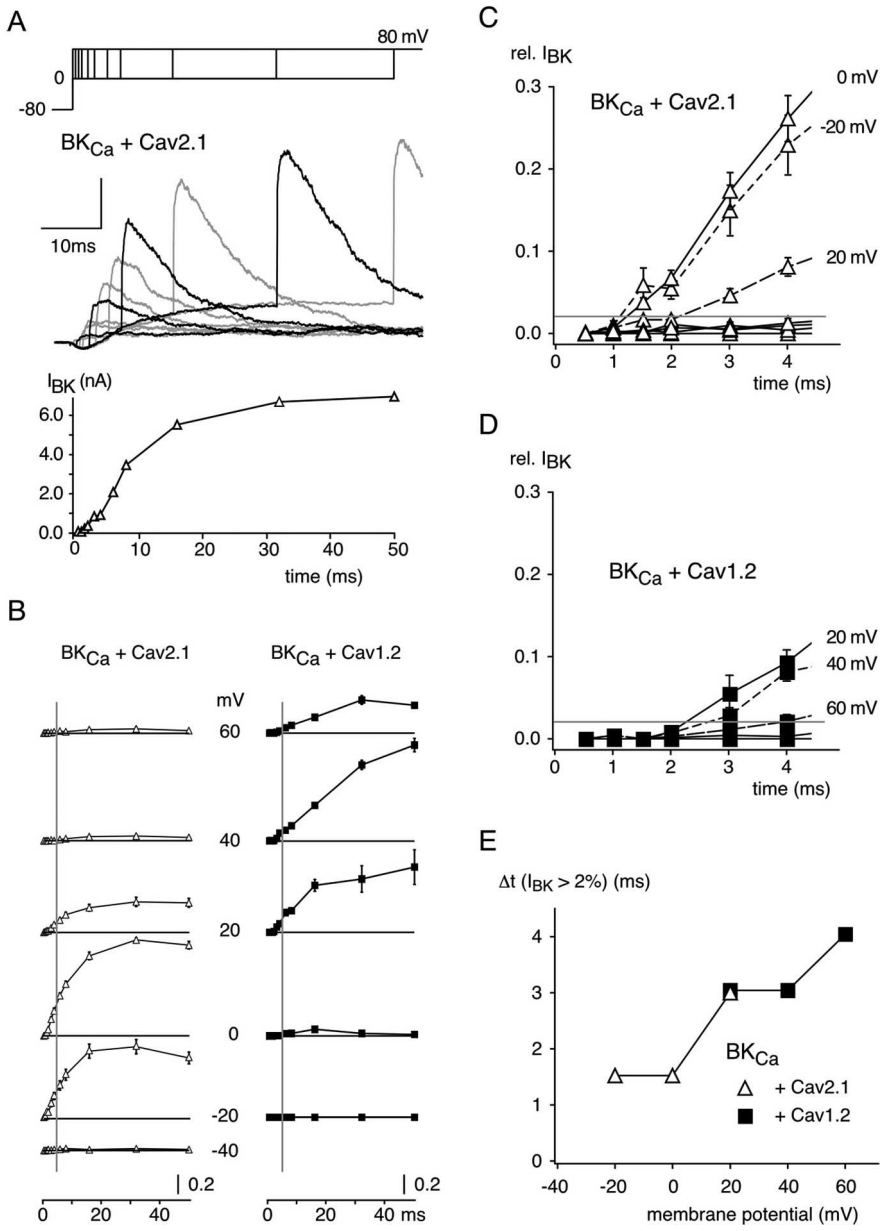


**Figure 2.** Time course of $K^+$ currents differs between $BK_{Ca}$–Cav2.1 and $BK_{Ca}$–Cav1.2 complexes. ***A***, Top, Middle, Currents through $BK_{Ca}$–Cav2.1 complexes recorded in inside-out (i–o) patches from oocytes in response to the indicated scanning tail-current protocol; steps to the tail potential (80 mV) were applied on top of a step depolarization to 0 mV at intervals of 0.5, 1, 1.5, 2, 3, 4, 6, 8, 16, 32, and 50 ms after the depolarization step. Current traces with tail steps at 1, 3, 8, and 32 ms are in black; the current scale is 2 nA. Bottom, Lot of $I_{tail}$ recorded in the experiment above as function of time. ***B***, Plot of normalized $I_{tail}$ recorded in experiments as in ***A*** in response to step depolarizations to the indicated voltages with $BK_{Ca}$–Cav2.1 (left) and $BK_{Ca}$–Cav1.2 complexes (right); individual experiments comprised the complete set of step depolarizations. $I_{tail}$ was normalized to the peak current recorded in each experiment. Data points are mean ± SEM of 13 and 7 experiments for $BK_{Ca}$–Cav2.1 and $BK_{Ca}$–Cav1.2 complexes, respectively. ***C***, ***D***, First 4 ms-period of the $I_{tail}$-plots from ***B*** (gray line in ***B***) at an enlarged scale. The horizontal bar denotes the 2% threshold. $BK_{Ca}$ currents under Cav2.1 (***C***) and Cav1.2 (***D***) from ***B***. For Cav2.1, voltage steps to −20, 0, and 20 mV evoked currents larger than the 2% threshold. For Cav1.2, voltage steps to 20, 40, and 60 mV evoked currents larger than the 2% threshold. Currents crossing the 2% threshold occurred within the first 2 ms after pulse start for $BK_{Ca}$ under Cav2.1, whereas $BK_{Ca}$ under Cav1.2 took longer than 2 ms to exceed the 2% at any voltage. ***E***, Summary plot of the lag phase [$\Delta t\,(I_{BK} > 2\%)$] defined by the interval between voltage step and $K^+$ current exceeding the 2% threshold for the two distinct $BK_{Ca}$–Cav complexes indicated. Note that $BK_{Ca}$ channels associated with Cav2.1 channels activated faster and at more negative potentials than those in complex with Cav1.2 channels.

and 24 ms generated repolarization (Fig. 4*A*, top). Figure 4*A* shows families of respective current responses recorded with Cav2.1 (middle) and Cav1.2 channels (bottom). With either channel, $Ca^{2+}$ currents were only measured during repolarization, whereas at the upstroke or the peak of the AP the $Ca^{2+}$ current was almost zero, similar to reports of Cav channels in CNS neurons (Raman and Bean, 1999; Bischofberger et al., 2002). Otherwise, the responses of the two Cav subtypes were greatly different, predominantly with respect to their time course as well as the time point of peak current amplitudes during a given AP. Thus, Cav2.1 channels exhibited the largest $Ca^{2+}$ currents for APs with half-widths ≤1 ms, whereas at longer APs the peak amplitudes successively decreased (Figs. 4*A*,*B*). In contrast, Cav1.2-mediated currents displayed maximal amplitudes at APs with half-widths ≥6.3 ms, whereas only approximately one-third of this peak level was obtained at short APs (half-widths ≤1) (Fig. 4*A*,*B*). Comparison of the time courses showed that AP-generated currents through Cav2.1 lasted longer and reached their peak amplitude significantly later than the currents mediated by Cav1.2 (Fig. 4*C*). Both observations are directly related to the different *I–V* relationships of Cav2.1 and Cav1.2 channels, as the time domain of the AP waveform command translates into progressive hyperpolarization of the membrane potential (Fig. 3*B*).

### Current responses of distinct $BK_{Ca}$–Cav complexes to AP waveform commands

Next, we investigated the $K^+$ current output of the two different $BK_{Ca}$–Cav complexes on AP waveform commands with a tail-current protocol scanning the time course of sole $BK_{Ca}$-mediated currents during the repolarization phase of the AP waveform (Fig. 5*A*, top). Figure 5*A* (middle) shows a typical family of $K^+$ current traces recorded from $BK_{Ca}$–Cav2.1 complexes during repolarization of an AP waveform with 6.34 ms half-duration. Thus, after a short lag phase, the $K^+$ currents (measured as instantaneous current amplitude at the tail step) increased to peak level and subsequently declined to zero toward the end of the AP waveform (Fig. 5*A*, bottom). Similar bell-shaped profiles were observed in all $K^+$ current responses of $BK_{Ca}$–Cav2.1 complexes to our set of AP waveform commands (half-width ranging from 1.02 to 12.24 ms), although both the current amplitude and the time-to-peak interval increased with increasing AP duration (Fig. 5*B*). Remarkably, the time-to-peak interval determined for the $K^+$ currents of $BK_{Ca}$–Cav2.1 complexes almost perfectly coincided with the respective interval obtained for $Ca^{2+}$ currents through Cav2.1 channels (Figs. 4*C*, 5*B*).

The current responses of $BK_{Ca}$–Cav1.2 channels to AP waveform commands were similar in their basic pattern to those of

their $BK_{Ca}$–Cav2.1 counterparts including the bell-shaped time course as well as the dependence of the time-to-peak interval and current amplitude on AP waveform duration (Fig. 5*B*). However, the distinct characteristics described above for the AP waveform responses of the two Cav channels alone (Fig. 4) were well preserved in the $K^+$ current responses of the two $BK_{Ca}$–Cav complexes. Thus, $K^+$ currents through $BK_{Ca}$–Cav2.1 complexes lasted longer and reached their peak amplitude considerably later than the $K^+$ currents mediated by $BK_{Ca}$–Cav1.2 complexes (Figs. 4*A*,*C*, 5*B*). In addition, pronounced differences between the two complexes were observed for $K^+$ currents generated by short AP waveforms with half-durations of 1.02 and 1.78 ms. Although $BK_{Ca}$ channels were effectively activated by these APs when associated with Cav2.1 channels, they either remained silent or were significantly less activated by the same AP waveforms when integrated into complexes with Cav1.2 (Fig. 5*C*,*D*).

Together, these results indicated that the $K^+$ current responses to AP waveform stimuli are distinct for the two different $BK_{Ca}$–Cav complexes mainly as a result of the distinct properties inherent to the respective Cav channel subtype.

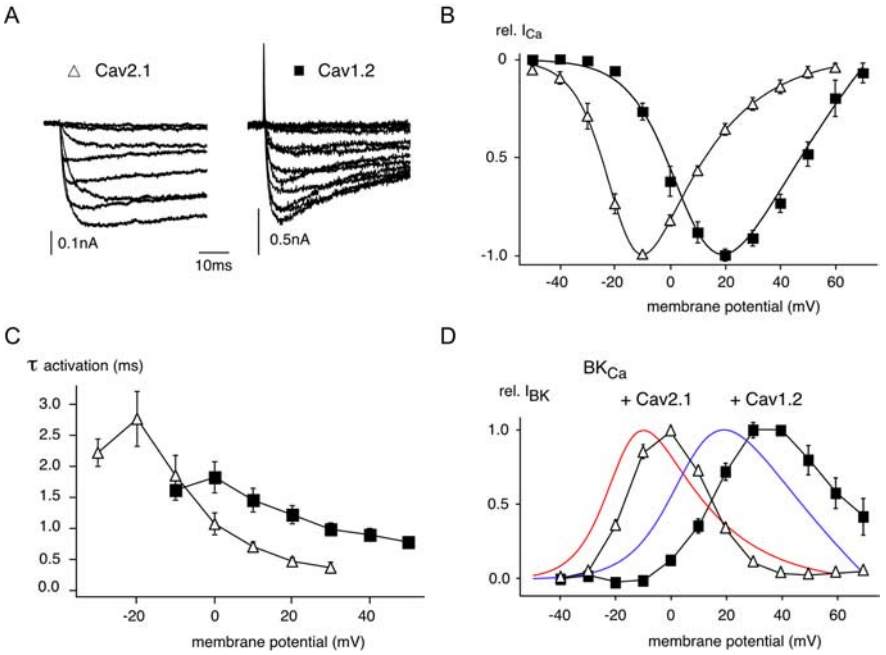


**Figure 3.** Distinct gating properties of Cav2.1 and Cav1.2 channels. ***A***, Currents mediated by Cav2.1 and Cav1.2 in response to voltage steps to potentials from −50 to 20 or 50 mV (10 mV increment) from a holding potential of −80 mV. Current and time scaling is as indicated. ***B***, Average *I–V* relationships of the two Cav channel subtypes determined from experiments as in ***A***. Data points are the mean ± SEM ($n = 9$ for Cav2.1; $n = 8$ for Cav1.2) of peak current amplitudes normalized to the maximal current. Continuous lines are fits of Equation 1 to the data. ***C***, Activation time constants ($\tau_{activation}$) derived from monoexponential fits to the onset of currents through Cav2.1 (open triangles, $n = 8$) or Cav1.2 channels (filled squares, $n = 8$). ***D***, Overlay of the *I–V* relationships of Cav2.1 (red) and Cav1.2 (blue) channels from ***B*** with the activation curves of $BK_{Ca}$ channels in complex with the respective Cav subtype (from Fig. 1*C*).

## Discussion

The central finding of the present work is that $K^+$ current responses of macromolecular $BK_{Ca}$–Cav complexes are mostly determined in both their voltage dependence and their time course by the $Ca^{2+}$ currents through the Cav subunit. The distinct gating properties of Cav2.1 (or P/Q-type channels) and Cav1.2 (or L-type channels) generated $BK_{Ca}$ currents with distinct profiles, particularly evident when complexes were operated by AP-like voltage commands. Whereas $BK_{Ca}$–Cav2.1 complexes responded robustly to short APs and provided repolarizing currents over almost the entire AP waveform, activation of $BK_{Ca}$ channels associated with Cav1.2 channels required longer APs and their currents declined far before the end of the AP waveform. These results establish the critical importance of the molecular composition of $BK_{Ca}$–Cav complexes and show how repolarizing responses of $BK_{Ca}$ channels can be adapted to distinct cellular requirements by association with distinct Cav subunits.

### Isolation of the $K^+$ current response of $BK_{Ca}$–Cav complexes

Functional analysis of $BK_{Ca}$–Cav complexes is hampered by the fact that any voltage command in the physiological range evokes combined $Ca^{2+}$ inward and $K^+$ outward currents. Because of their opposite direction, both currents distort or cancel each other when their amplitudes are similar in size, which occurs in both heterologous expression systems and native cells at voltages around the activation threshold of the $BK_{Ca}$ channels or in responses to AP waveform commands (Figs. 2, 5). Because membrane depolarization elicits $Ca^{2+}$ currents in Cav channels forming complexes with $BK_{Ca}$, but also in complex-free channels, the $Ca^{2+}$ current amplitude may equal that of $BK_{Ca}$ currents, despite the markedly smaller conductance of the Cav channels.

For characterization of isolated $BK_{Ca}$-mediated $K^+$ currents we, therefore, used scanning tail-current protocols that circumvent the problem of interfering current components: by tail steps to the $Ca^{2+}$ reversal potential, these protocols cancel the $Ca^{2+}$ currents and, at the same time, enhance the $K^+$ currents to be investigated (because of the increased driving force for $K^+$ ions) (Prakriya and Lingle, 1999; Yazejian et al., 2000). Thus, this strategy offers two major advantages: (1) it detects $BK_{Ca}$ channel activity even at the low levels observed around their activation threshold or in response to the brief $Ca^{2+}$ currents generated by APs; (2) this detection is not affected by the superimposing $Ca^{2+}$ currents.

Consequently, the scanning tail-current protocols enabled the precise determination of $BK_{Ca}$ channel activity with voltage steps as well as with dynamic AP waveform commands.

### Operation of $BK_{Ca}$–Cav complexes: control of $K^+$ channel activity by the Cav partner

The functional properties of $BK_{Ca}$ channels were greatly different when integrated into bimolecular complexes with either Cav2.1 or Cav1.2 channels, the Cav channels encoding P/Q- and L-type channels, respectively (Fig. 1, 2). Most prominently, the steady-state activation curve of $BK_{Ca}$ channels fueled by coassembled Cav2.1 rose and declined at markedly more negative potentials (Fig. 1*C*), and the onset of their $K^+$ currents was faster by approximately a factor of twofold (Figs. 2*C–E*). Both of these differences are paralleled by the differences observed for the activation time course and *I–V* relationship of the $Ca^{2+}$ currents mediated by the two different Cav channel subtypes. Thus, the bell-shaped *I–V* relationship of Cav2.1 channels was positioned negative to that of Cav1.2

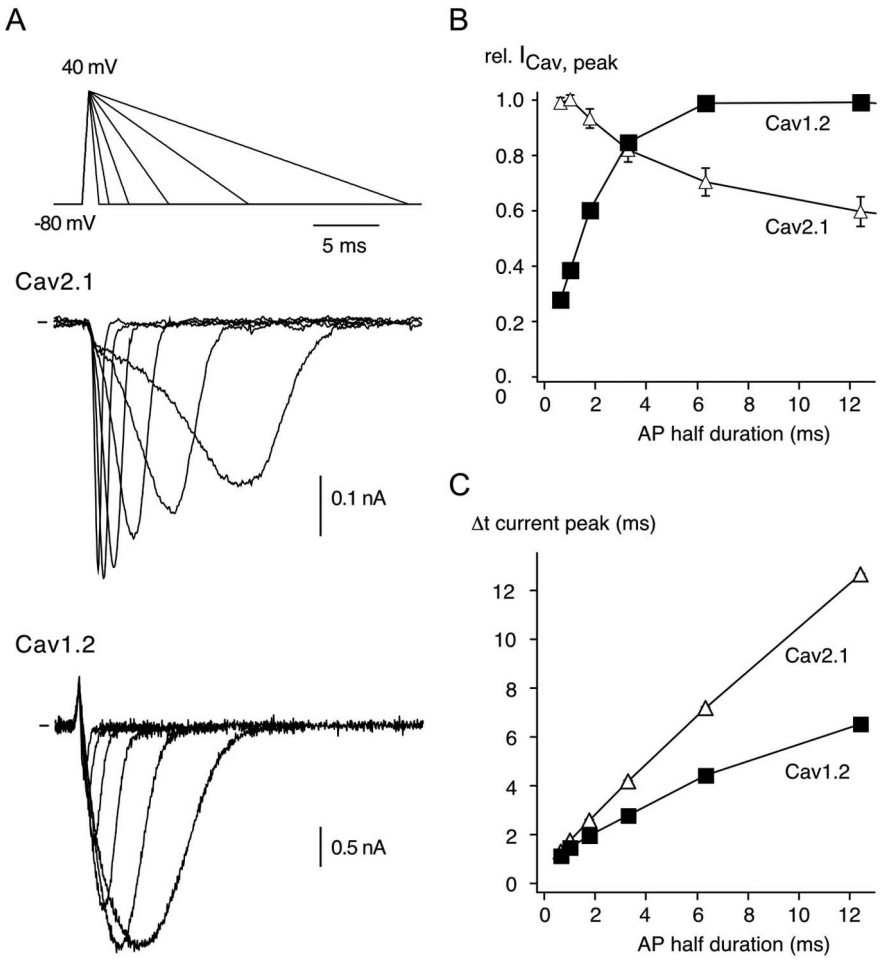


**Figure 4.** Current responses of Cav2.1 and Cav1.2 channels to AP stimuli. ***A***, Representative current traces evoked in Cav2.1 (middle) and Cav1.2 (bottom) channels by AP-like waveforms (top) comprising a 0.52 ms depolarizing ramp from −80 to 40 mV and a repolarizing ramp from 40 to −80 mV with variable duration of 0.76, 1.52, 3.04, 6.08, 12.16, or 24.32 ms; these durations correspond to AP half durations of 0.64, 1.02, 1.78, 3.3, 6.34, and 12.42 ms. Note the distinct current profiles generated by the two Cav subtypes. ***B***, Peak $Ca^{2+}$ currents elicited by AP-like waveforms normalized to the maximal current amplitude obtained with the AP series indicated in ***A***. Data points are the mean ± SEM of six experiments for each Cav channel. ***C***, Period between peak current and start of the AP command ($\Delta t_{peak\ current}$) as a function of the AP half duration. Data points are mean ± SEM of six experiments for each Cav channel. Note the distinct increase in $\Delta t_{peak\ current}$ for both Cav subtypes.

on the voltage axis (Fig. 3*B*), and the $\tau_{activation}$ for Cav2.1 exhibited approximately half the value of the $\tau_{activation}$ for Cav1.2 (Fig. 3*C*). These findings establish the $Ca^{2+}$ currents through the coassembled Cav partner as the major determinant of $BK_{Ca}$ channel gating in $BK_{Ca}$–Cav complexes under steady-state conditions.

However, $BK_{Ca}$ channel activity is not exclusively shaped by the $Ca^{2+}$ current as visualized by the deviations of the $BK_{Ca}$ activation curves from the Cav channel *I–V* relationships (Fig. 3*D*). At voltages in the "rising phase" of the Cav channel *I–V* relationship, $BK_{Ca}$ channels were less active than anticipated from the $Ca^{2+}$ current amplitude, whereas in its "falling phase" $BK_{Ca}$ channel activity exceeded the respective predictions. In either case, the discrepancy most likely results from the gating properties of both $BK_{Ca}$ and Cav channels. In particular, the higher $BK_{Ca}$ activity in the voltage range of decreasing $Ca^{2+}$ currents is likely attributable to the unique gating mechanism of $BK_{Ca}$ channels in which decreasing $[Ca^{2+}]_i$ can be compensated by increasingly positive membrane potentials. Thus, in addition to the $Ca^{2+}$ currents, the gating characteristics of both Cav and $BK_{Ca}$ channels participate in shaping the $K^+$ current output of $BK_{Ca}$–Cav complexes under steady-state conditions.

Considering $BK_{Ca}$ as an attached sniffer for $Ca^{2+}$ ions (Berkefeld et al., 2006), the overlays in Figure 3*D* emphasize an interesting difference in the *I–V* relationships of the two Cav channel subtypes used. Cav2.1-mediated $Ca^{2+}$ currents steeply decrease at voltages >0 mV (as do $BK_{Ca}$-mediated $K^+$ currents), although the open probabilities of the channels are maximal in this voltage range and the driving force for $Ca^{2+}$ ions is sufficiently high to promote robust currents, as evident from the contrasting results obtained with Cav1.2 channels and $BK_{Ca}$–Cav1.2 complexes. How this phenomenon is brought about is unclear.

### Tuning repolarizing AP responses by distinct Cav subunits

When subjected to dynamic voltage commands with AP-like waveforms, the distinct gating properties of Cav1.2 and Cav2.1 (Fig. 3) shaped $Ca^{2+}$ currents with particular properties (Fig. 4). Whereas Cav1.2 promoted rapidly peaking currents that require long-lasting AP waveforms to reach their maximal amplitude, Cav2.1 channels reliably responded even to submillisecond AP waveforms and were active over almost the entire length of the AP waveform. In complexes with $BK_{Ca}$ channels, the distinct characteristics of the two Cav subtypes translated into $K^+$ currents that almost perfectly mirrored the respective $Ca^{2+}$ current input (Fig. 5). Thus, responses to short AP waveforms were only observed with $BK_{Ca}$ channels coassembled with Cav2.1, whereas longer AP waveforms evoked robust currents in both $BK_{Ca}$–Cav2.1 and $BK_{Ca}$–Cav1.2 complexes, although with mostly distinct time courses (Fig. 5*B–D*).

These findings for $BK_{Ca}$–Cav complexes with different subunit compositions should impact native cells in several ways. First, they explain why $BK_{Ca}$-mediated $K^+$ currents can be quite different among different types of cell (Edgerton and Reinhart, 2003; Jackson et al., 2004). Second, they illustrate how $BK_{Ca}$-mediated repolarizations may be adapted in both time course and amplitude to the distinct cellular requirements via the expression pattern of Cav channels. Accordingly, in cells with fast APs and/or millisecond fAHPs, $BK_{Ca}$ channels should be preferentially associated with Cav2.1 channels, whereas in cells with longer-lasting APs, Cav1.2 channels or both Cav subtypes would be expected as partners of $BK_{Ca}$. This has indeed been observed. Thus, in cerebellar Purkinje cells where narrow spikes are found together with pronounced fAHPs, $BK_{Ca}$ channels are predominantly fueled by P/Q-type channels (Edgerton and Reinhart, 2003; Womack et al., 2004), whereas in chromaffin or smooth muscle cells, where APs are typically as long as a few milliseconds, $BK_{Ca}$ channels were found to partner with both Cav1.2 and Ca2.1 channels (Prakriya and Lingle, 1999; Berkefeld et al., 2006).

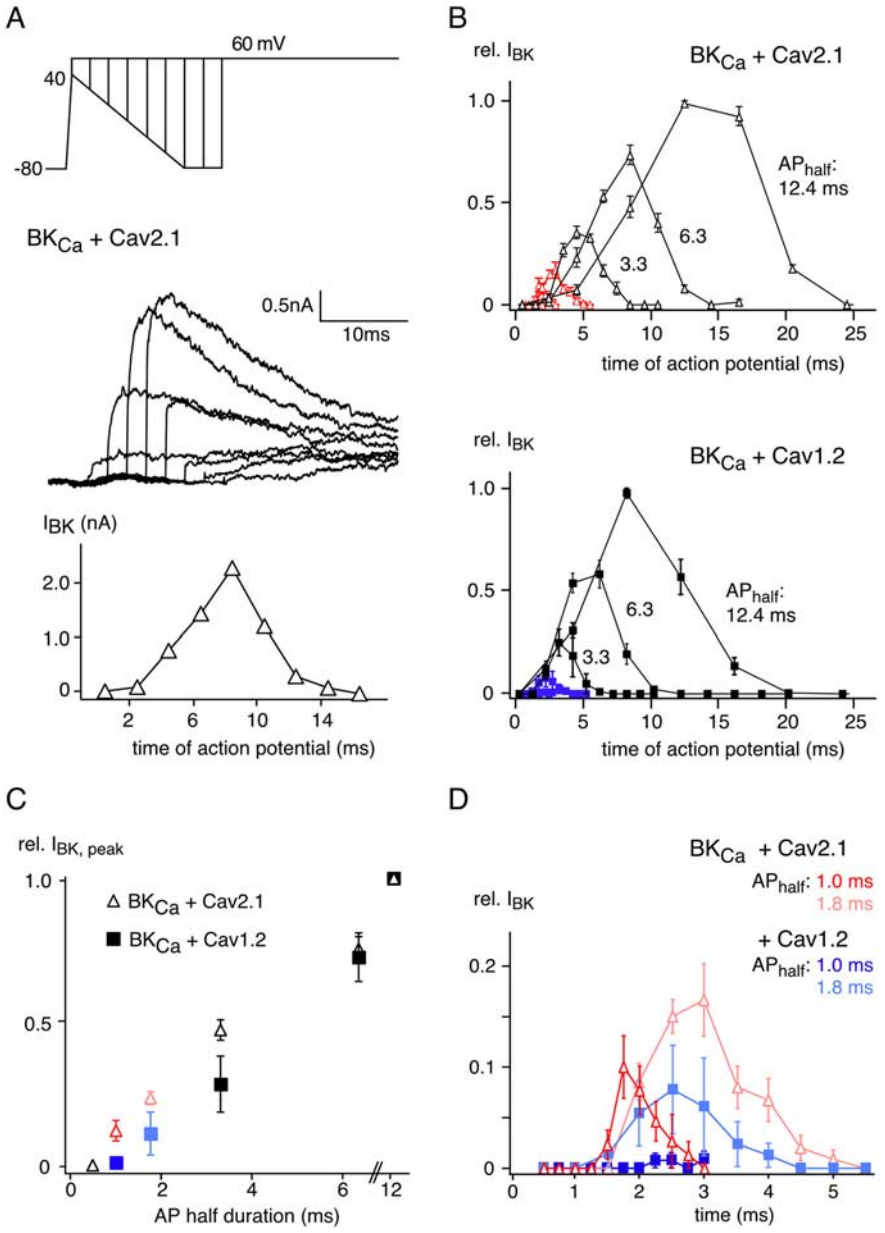


**Figure 5.** Differential responses of $BK_{Ca}$–Cav2.1 and $BK_{Ca}$–Cav1.2 complexes to AP stimuli. ***A***, Top, Middle, Family of $K^+$ current traces recorded from $BK_{Ca}$–Cav2.1 complexes in an individual (i–o) patch in response to the scanning tail protocol indicated. Activation of the $BK_{Ca}$ channels along the AP repolarization was determined by equally spaced tail steps to 60 mV. Time and current scaling as indicated. Bottom, $I_{tail}$ plotted over time of AP (origin is the start of the AP). ***B***, Plots of $I_{tail}$ obtained with a series of APs of variable half-width (as given in Fig. 4) applied to $BK_{Ca}$–Cav2.1 (top) and BKCa–Cav1.2 channels (bottom); currents were normalized to the peak amplitude obtained with an AP of 12.4 ms half-width. Data points are mean ± SEM of five and seven experiments, respectively. ***C***, Summary of normalized peak $K^+$ current amplitudes determined for $BK_{Ca}$–Cav2.1 (triangles) and $BK_{Ca}$–Cav1.2 (squares) complexes in the experiments in ***B*** as a function of AP half duration. Color coding is as in ***D***. ***D***, $I_{tail}$ plots of $BK_{Ca}$–Cav2.1 (lines and triangles in red) and $BK_{Ca}$–Cav1.2 (lines and squares in blue) complexes determined with short APs of 1.02 and 1.78 ms half-durations.

## References


Augustine GJ, Santamaria F, Tanaka K (2003) Local calcium signaling in neurons. Neuron 40:331–346.

Berkefeld H, Sailer CA, Bildl W, Rohde V, Thumfart JO, Eble S, Klugbauer N, Reisinger E, Bischofberger J, Oliver D, Knaus HG, Schulte U, Fakler B (2006) $BK_{Ca}$-Cav channel complexes mediate rapid and localized $Ca^{2+}$-activated $K^+$ signaling. Science 314:615–620.

Bildl W, Strassmaier T, Thurm H, Andersen J, Eble S, Oliver D, Knipper M, Mann M, Schulte U, Adelman JP, Fakler B (2004) Protein kinase CK2 is coassembled with small conductance $Ca^{2+}$-activated $K^+$ channels and regulates channel gating. Neuron 43:847–858.

Bischofberger J, Geiger JR, Jonas P (2002) Timing and efficacy of $Ca^{2+}$ channel activation in hippocampal mossy fiber boutons. J Neurosci 22:10593–10602.

Castillo PE, Weisskopf MG, Nicoll RA (1994) The role of $Ca^{2+}$ channels in hippocampal mossy fiber synaptic transmission and long-term potentiation. Neuron 12:261–269.

Cui J, Cox DH, Aldrich RW (1997) Intrinsic voltage dependence and $Ca^{2+}$ regulation of mslo large conductance Ca-activated $K^+$ channels. J Gen Physiol 109:647–673.

Dobremez E, Bouali-Benazzouz R, Fossat P, Monteils L, Dulluc J, Nagy F, Landry M (2005) Distribution and regulation of L-type calcium channels in deep dorsal horn neurons after sciatic nerve injury in rats. Eur J Neurosci 21:3321–3333.

Edgerton JR, Reinhart PH (2003) Distinct contributions of small and large conductance $Ca^{2+}$-activated $K^+$ channels to rat Purkinje neuron function. J Physiol 548:53–69.

Fakler B, Brändle U, Glowatzki E, Weidemann S, Zenner HP, Ruppersberg JP (1995) Strong voltage-dependent inward rectification of inward rectifier $K^+$ channels is caused by intracellular spermine. Cell 80:149–154.

Golding NL, Jung HY, Mickus T, Spruston N (1999) Dendritic calcium spike initiation and repolarization are controlled by distinct potassium channel subtypes in CA1 pyramidal neurons. J Neurosci 19:8789–8798.

Heppner TJ, Bonev AD, Nelson MT (1997) $Ca^{2+}$-activated $K^+$ channels regulate action potential repolarization in urinary bladder smooth muscle. Am J Physiol 273:C110–C117.

Hu H, Shao LR, Chavoshy S, Gu N, Trieb M, Behrens R, Laake P, Pongs O, Knaus HG, Ottersen OP, Storm JF (2001) Presynaptic $Ca^{2+}$-activated $K^+$ channels in glutamatergic hippocampal terminals and their role in spike repolarization and regulation of transmitter release. J Neurosci 21:9585–9597.

Jackson AC, Yao GL, Bean BP (2004) Mechanism of spontaneous firing in dorsomedial suprachiasmatic nucleus neurons. J Neurosci 24:7985–7998.

Kulik A, Nakadate K, Hagiwara A, Fukazawa Y, Luján R, Saito H, Suzuki N, Futatsugi A, Mikoshiba K, Frotscher M, Shigemoto R (2004) Immunocytochemical localization of the alpha 1A subunit of the P/Q-type calcium channel in the rat cerebellum. Eur J Neurosci 19:2169–2178.

Lancaster B, Nicoll RA (1987) Properties of two calcium-activated hyperpolarizations in rat hippocampal neurones. J Physiol 389:187–203.

Latorre R, Brauchi S (2006) Large conductance $Ca^{2+}$-activated $K^+$ (BK) channel: activation by $Ca^{2+}$ and voltage. Biol Res 39:385–401.

Loane DJ, Lima PA, Marrion NV (2007) Co-assembly of N-type $Ca^{2+}$ and BK channels underlies functional coupling in rat brain. J Cell Sci 120:985–995.

Lovell PV, McCobb DP (2001) Pituitary control of BK potassium channel function and intrinsic firing properties of adrenal chromaffin cells. J Neurosci 21:3429–3442.

Marty A (1981) Ca-dependent K channels with large unitary conductance in chromaffin cell membranes. Nature 291:497–500.

Müller A, Kukley M, Uebachs M, Beck H, Dietrich D (2007) Nanodomains of single $Ca^{2+}$ channels contribute to action potential repolarization in cortical neurons. J Neurosci 27:483–495.

Neher E (1998) Vesicle pools and $Ca^{2+}$ microdomains: new tools for understanding their roles in neurotransmitter release. Neuron 20:389–399.

Obermair GJ, Szabo Z, Bourinet E, Flucher BE (2004) Differential targeting of the L-type $Ca^{2+}$ channel alpha 1C (CaV1.2) to synaptic and extrasynaptic compartments in hippocampal neurons. Eur J Neurosci 19:2109–2122.

Pattillo JM, Yazejian B, DiGregorio DA, Vergara JL, Grinnell AD, Meriney SD (2001) Contribution of presynaptic calcium-activated potassium currents to transmitter release regulation in cultured *Xenopus* nerve-muscle synapses. Neuroscience 102:229–240.

Pelkey KA, Topolnik L, Lacaille JC, McBain CJ (2006) Compartmentalized $Ca^{(2+)}$ channel regulation at divergent mossy-fiber release sites underlies target cell-dependent plasticity. Neuron 52:497–510.

Prakriya M, Lingle CJ (1999) BK channel activation by brief depolarizations requires $Ca^{2+}$ influx through L- and Q-type $Ca^{2+}$ channels in rat chromaffin cells. J Neurophysiol 81:2267–2278.

Raman IM, Bean BP (1999) Ionic currents underlying spontaneous action potentials in isolated cerebellar Purkinje neurons. J Neurosci 19:1663–1674.

Rancz EA, Häusser M (2006) Dendritic calcium spikes are tunable triggers of cannabinoid release and short-term synaptic plasticity in cerebellar Purkinje neurons. J Neurosci 26:5428–5437.

Reid CA, Bekkers JM, Clements JD (2003) Presynaptic $Ca^{2+}$ channels: a functional patchwork. Trends Neurosci 26:683–687.

Robitaille R, Garcia ML, Kaczorowski GJ, Charlton MP (1993) Functional colocalization of calcium and calcium-gated potassium channels in control of transmitter release. Neuron 11:645–655.

Sah P, Faber ES (2002) Channels underlying neuronal calcium-activated potassium currents. Prog Neurobiol 66:345–353.

Shao LR, Halvorsrud R, Borg-Graham L, Storm JF (1999) The role of BK-type $Ca^{2+}$-dependent $K^+$ channels in spike broadening during repetitive firing in rat hippocampal pyramidal cells. J Physiol 521:135–146.

Storm JF (1987a) Intracellular injection of a $Ca^{2+}$ chelator inhibits spike repolarization in hippocampal neurons. Brain Res 435:387–392.

Storm JF (1987b) Action potential repolarization and a fast after-hyperpolarization in rat hippocampal pyramidal cells. J Physiol 385:733–759.

Ukhanov K, Leinders-Zufall T, Zufall F (2007) Patch-clamp analysis of gene-targeted vomeronasal neurons expressing a defined V1r or V2r receptor: ionic mechanisms underlying persistent firing. J Neurophysiol 98:2357–2369.

Womack MD, Chevez C, Khodakhah K (2004) Calcium-activated potassium channels are selectively coupled to P/Q-type calcium channels in cerebellar Purkinje neurons. J Neurosci 24:8818–8822.

Wu LG, Westenbroek RE, Borst JG, Catterall WA, Sakmann B (1999) Calcium channel types with distinct presynaptic localization couple differentially to transmitter release in single calyx-type synapses. J Neurosci 19:726–736.

Yazejian B, Sun XP, Grinnell AD (2000) Tracking presynaptic $Ca^{2+}$ dynamics during neurotransmitter release with $Ca^{2+}$-activated $K^+$ channels. Nat Neurosci 3:566–571.